This article has been accepted for publication in IEEE Networking Letters. This is the author's version which has not been fully edited and content may change prior to final publication. Citation information: DOI 10.1109/LNET.2026.3737598

Dynamic RIS Partitioning in Downlink NOMA Systems based on Quality of Service Optimization

Luca Pallotta, *Senior Member, IEEE*

***Abstract*—The integration of reconfigurable intelligent surfaces (RIS) with non-orthogonal multiple access (NOMA) is a promising solution for improving connectivity and spectral efficiency in next-generation wireless networks. However, joint optimization of all RIS elements could be computationally challenging. This letter proposes a quality of service (QoS)-driven RIS partitioning for downlink RIS-assisted NOMA systems. Herein, the RIS is dynamically divided into sub-surfaces assigned to different user subsets. User requirements are captured through utility functions, and the resulting constrained optimization problem is solved numerically to maximize system performance. Numerical results confirm the effectiveness of the proposed RIS partitioning strategy.**

***Index Terms*—non-orthogonal multiple access (NOMA), reconfigurable intelligent surfaces (RIS), RIS partitioning, quality-of-service (QoS) optimization.**

I. INTRODUCTION

THE evolution toward sixth-generation (6G) wireless networks entails increased system complexity and resource demands, driven by the need to support integrated communication and sensing functionalities [1]. In this context, non-orthogonal multiple access (NOMA) and reflective intelligent surfaces (RIS) have emerged as key enabling technologies to enhance quality-of-service (QoS), spectral efficiency, and massive connectivity. Unlike conventional schemes, power-domain NOMA (P-NOMA) allows multiple users to share the same time-frequency resources through power multiplexing [2], [3]. In downlink transmissions, higher power is allocated to users with weaker channel conditions, while users with stronger channels apply successive interference cancellation (SIC) to decode and cancel weaker users' signals before detecting their own. Meanwhile, a RIS comprises a large number of reconfigurable elements that manipulate incident signals via adjustable phase shifts, thereby shaping the propagation environment and enabling virtual line of sight (LOS) links even under blockage conditions [4], [5].

Several studies have investigated the integration of RIS into NOMA-based communication systems [6]–[11]. However, jointly optimizing all RIS elements in large-scale deployments results in high computational complexity and increased processing latency. To address this challenge, RIS partitioning has emerged as an effective solution by dividing the array into multiple sub-surfaces, thereby enabling more tractable optimization, mitigating interference in non line of sight (NLOS) scenarios, and supporting high-performance communications [12]–[18]. Despite these advances, existing RIS partitioning approaches mainly focus on beamforming optimization, or learning-based partitioning strategies. Furthermore, RIS partitioning strategies in NOMA systems are typically limited to two-user settings and seldom address QoS-aware resource allocation in scalable downlink multi-user systems.

Motivated by the above limitations, this paper proposes a QoS-driven resource allocation framework for downlink RIS-assisted multi-user NOMA systems based on dynamic logical RIS partitioning. Specifically, logical RIS sub-surfaces are dynamically assigned to individual users, reducing the optimization complexity and mitigating inter-user interference in NLOS scenarios. Utility functions are introduced to model heterogeneous QoS requirements, and the resource allocation problem is formulated, following the line of reasoning of [19]–[21], as a constrained optimization problem aimed at maximizing the overall system utility. The resulting optimization problem is non-convex and available only in implicit form, thus requiring numerical optimization techniques to obtain practical solutions. Numerical simulations demonstrate the effectiveness of the proposed framework, showing that dynamic power-aperture product (PAP) allocation provides higher system utility and a fairer distribution of spectral efficiency than a conventional static allocation strategy under heterogeneous QoS requirements.

The letter is organized as follows. Section II introduces the downlink RIS-assisted NOMA system and formulates the QoS optimization problem with RIS partitioning. Section III presents the user quality metric together with the proposed solution. Section IV evaluates the effectiveness of the approach through simulations. Finally, Section V concludes the letter and suggests possible future researches.

II. PROBLEM FORMULATION

A RIS-assisted downlink P-NOMA system serving multiple users under a QoS-driven RIS partitioning framework is considered. The system comprises a base station (BS), a RIS shaped as a uniform rectangular array (URA) equipped with $N = N_x \times N_y$ reflecting elements, and K single-antenna NOMA users, as illustrated in Fig. 1. Obstacles are assumed to block the direct BS-user links, forcing communication to occur exclusively through RIS-reflected links.

The proposed downlink framework employs SIC for user separation while dynamically partitioning the RIS to control

L. Pallotta is with the Department of Engineering (DiING), University of Basilicata, via dell'Ateneo Lucano 10, 85100 Potenza, Italy. E-mail: luca.pallotta@unibas.it.
This work is funded by the Italian Ministry of University and Research (MUR) through the Italian program "Bando PRIN 2022," D.D. 104/2022, Project "Intelligent Reflecting Surfaces Application to NOMA Systems" ("INTRIGANTE"), Grant number 20225CC9RW, CUP C53C24000780006. This manuscript reflects only the author's views and opinions, and the Ministry cannot be considered responsible for them.

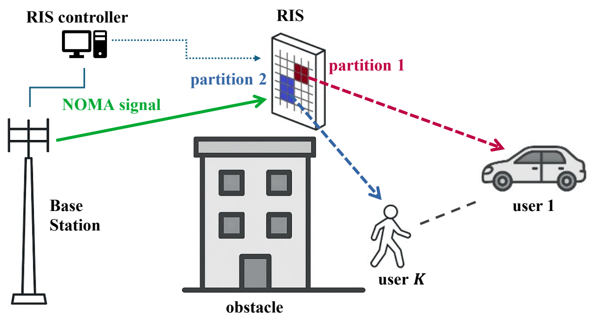

Fig. 1. Notional representation of the considered RIS-assisted downlink NOMA communication system.

the allocation of PAP to each user[1]. Specifically, disjoint subsets of RIS elements are assigned to different users, forming clusters whose aggregate PAP can be tailored to meet individual QoS requirements. When sufficient PAP is available, each user can receive the amount required to achieve its target QoS; otherwise, the total available PAP is dynamically shared among the K NOMA users. Each user U_i exploits the allocated PAP_i to achieve a specific QoS, quantified by a quality metric $q_i(PAP_i)$. These quality metrics are mapped into utility functions that measure the satisfaction level associated with the achieved performance. The RIS controller determines the optimal PAP partition by maximizing a weighted sum of individual utilities, thereby accounting for heterogeneous service requirements and user priorities. Letting $\boldsymbol{PAP} = [PAP_1, \ldots, PAP_K]^T$, the optimal RIS partitioning is realized as the solution to the following constrained optimization problem [19], [21], [22]

$$\mathcal{P}\left\{\begin{array}{ll} & \max\limits_{\boldsymbol{PAP}} u(\boldsymbol{PAP}) = \sum\limits_{i=1}^{K} w_i u_i(q_i(PAP_i)) \\ \text{s.t.} & \sum\limits_{i=1}^{K} PAP_i \leq PAP_{tot} \\ & PAP_i \geq PAP_{\min_i}, i = 1, \ldots, K \end{array}\right. , \quad (1)$$

with PAP_{tot} the total available PAP at the RIS, whereas $u_i(\cdot)$, and w_i, $i = 1, \ldots, K$, are the utility function and the priority weight associate to the i-th user. Finally, $PAP_{\min_i}$, $i = 1, \ldots, K$, guarantees that the i-th user's communication is performed with a minimum QoS level.

Notice that, if the utility function $u_i\left(q_i(PAP_i)\right)$ is continuous and convex in PAP_i, the overall objective is convex and the optimal allocation can be derived from the Karush-Kuhn-Tucker (KKT) conditions [19, Chap. 5]. In the considered RIS partitioning framework, however, the quality metric lacks a closed-form expression, making the optimization problem only numerically tractable. Moreover, although Problem $\mathcal{P}$ shares the same mathematical structure as the formulations in [19], [21], [22], it differs substantially because it is based on a different quality metric.

[1] The PAP is defined as the product of the average transmitted power and the effective antenna aperture.

III. Quality metric and utility for RIS partitioning

The allocation strategy in Problem $\mathcal{P}$ relies on the figures of merit $q_i(\cdot;\cdot)$ and utility functions $u_i(\cdot)$, $i = 1, \ldots, K$. This section defines these quantities to explicitly characterize the proposed RIS-partitioning framework.

A. P-NOMA communication range with RIS-PAP allocation

In this P-NOMA context, the considered quality metric is the maximum communication range $R^\star$ at which the achieved spectral efficiency meets a prescribed value $C^\star$. Transmission relies on the superposition of power-domain signals, which inherently introduces intra-cluster interference analyzed in terms of signal to interference plus noise ratio (SINR).

Before evaluating $R^\star$, consider a BS transmitting a superposition of non-orthogonal waveforms $x_i(t)$, $i = 1, \ldots, K$, to K P-NOMA users through a RIS, where each waveform is weighted by a power coefficient P_i. Assuming an additive white Gaussian noise (AWGN) channel, after matched filtering with respect to $x_k(t)$ and sampling, the received signal at user k is given by

$$r_k = \sqrt{P_k}\,\beta_k g_k \alpha_k + I_k + w_k, \quad (2)$$

where g_k denotes the RIS beamforming gain and

$$I_k = \beta_k g_k \sum_{j \neq k} \sqrt{P_j}\alpha_j \quad (3)$$

represents the intra-cluster interference from other NOMA users. Here, β_k models the RIS-user channel propagation and receive antenna effects, and α_k denotes the information symbol of user k, satisfying the unit-power constraint $\mathbb{E}\{|\alpha_k|^2\} = 1$. The additive noise term w_k is modeled as complex Gaussian with zero mean and variance σ_k^2.

It is worth recalling that, in downlink P-NOMA, users are ordered according to their channel quality, with higher transmission power allocated to users experiencing weaker channels. Consequently, users with better channel conditions perform SIC by successively decoding and removing the signals intended for users with weaker channels before decoding their own signal. Therefore, after interference cancellation, the residual interference experienced by user k originates only from the signals intended for users with better channel conditions, namely those indexed by $j > k$ under an ascending channel-quality ordering. Accordingly, the SINR at user k is given by

$$\gamma_k = \frac{P_k |g_k|^2 \, |\beta_k|^2}{\sum\limits_{j=k+1}^{K} P_j |g_k|^2 \, |\beta_k|^2 + \sigma_k^2}, \quad (4)$$

where the summation term in the denominator accounts for the residual interference from users that have not yet been canceled; moreover, $\sigma_k^2 = k_B T_s B$ is the noise power at the k-th receiver, with T_s and B the respective noise system temperature and effective bandwidth.

Let us observe now that [21]

$$P_k |g_k|^2 \, |\beta_k|^2 = P_k \frac{G_T A_e^{\mathrm{rx},k}}{4\pi R_k^2 L_s} \quad (5)$$

with $A_e^{\mathrm{rx},k}$ the effective area of the k-th user receiving antenna, G_T is the transmitting antenna gain, and L_s the total system loss. Hence, following the above definitions, γ_k in (4) can be expressed as

$$\gamma_k = \frac{P_k \frac{G_T A_e^{\mathrm{rx},k}}{4\pi R_k^2 L_s}}{\sum_{j=k+1}^{K} P_j \frac{G_T A_e^{\mathrm{rx},k}}{4\pi R_k^2 L_s} + \sigma_k^2}. \tag{6}$$

In order to jointly account for transmit power allocation and RIS aperture, the PAP allocated at the RIS to the k-th user is introduced, that is

$$PAP_k \triangleq P_k A_{\mathrm{RIS}}, \tag{7}$$

where A_{RIS} is the effective RIS aperture. As a consequence, the SINR for the k-th user under P-NOMA with SIC in (6) becomes

$$\gamma_k = \frac{\frac{PAP_k A_e^{\mathrm{rx},k}}{\lambda^2 R_k^2 L_s}}{\sum_{j=k+1}^{U} \frac{PAP_j A_e^{\mathrm{rx},k}}{\lambda^2 R_k^2 L_s} + \sigma_k^2} = \frac{PAP_k}{\sum_{j=k+1}^{U} PAP_j + \frac{\lambda^2 R_k^2 L_s}{A_e^{\mathrm{rx},k}} \sigma_k^2}, \tag{8}$$

with λ the operating wavelength.

Finally, the spectral efficiency (in bps/Hz) of user k is expressed as [23]

$$C_k = \log_2(1+\gamma_k). \tag{9}$$

By imposing a target spectral efficiency $C^\star$, i.e., $C_k = C^\star$, the corresponding SINR requirement can be obtained as

$$\gamma^\star = 2^{C^\star} - 1. \tag{10}$$

Substituting $\gamma_k = \gamma^\star$ into (8) and solving for R_k, the maximum communication range for the k-th user becomes

$$R_k^\star = \sqrt{\frac{A_e^{\mathrm{rx},k}}{\lambda^2 L_s \sigma_k^2}\left(\frac{PAP_k}{\gamma^\star} - \sum_{j=k+1}^{U} PAP_j\right)}. \tag{11}$$

This expression explicitly shows how the maximum communication range depends on the RIS aperture, the allocated power, the residual P-NOMA interference, and the receiver characteristics, providing a direct link between physical resources and achievable spectral efficiency. Finally, it is worth noting that, when the number of users becomes large, the proposed methodology can be extended to consider grouped or clustered users, with each group associated with a subsurface or a set of resource units. This strategy would reduce the dimensionality of the optimization problem in large-scale scenarios. Exploring this extension is left for future work.

B. Utility function and optimization algorithm

Once the quality metrics are defined, the optimal allocation of PAPs among the NOMA users is obtained by solving the QoS optimization Problem $\mathcal{P}$. In this framework, the RIS controller maps the quality metrics into utility functions that quantify the satisfaction level of individual users. Accordingly, the utility of user i is modeled as a non-linear function of its associated quality metric [24], [25]

$$u_i(R) = \begin{cases} 0, & R < R_{t_i} \\ \left(\frac{R-R_{t_i}}{R_{o_i}-R_{t_i}}\right)^{\xi_i}, & R_{t_i} \le R \le R_{o_i} \\ 1, & R > R_{o_i} \end{cases}. \tag{12}$$

Here, R_{t_i} and R_{o_i} are the threshold and objective ranges for the i-th user, respectively, and R denotes the target communication range $R^\star$. The exponent ξ_i controls the curvature of the utility function. In fact, $\xi_i > 1$ emphasizes values close to the objective, whereas $0 < \xi_i < 1$ gives a faster initial increase.

Now, to solve the challenging, non-convex RIS partitioning Problem $\mathcal{P}$, the iterative optimization algorithm proposed in [26] is employed. The algorithm uses an interior-point approach, which addresses a sequence of approximate problems with non-negativity-constrained slack variables and equality constraints. These approximate problems are easier to solve than the original inequality-constrained formulation and can be tackled either by directly solving the associated KKT conditions via a linear (Newton) step or using a conjugate gradient method [27].

IV. PERFORMANCE ANALYSIS

In this section, the effectiveness of the proposed approach is validated through simulations, where as in [21], Problem $\mathcal{P}$ is solved using the MathWorks MATLAB® *Quality-of-Service Optimization for Radar Resource Management* tool [22], which performs constrained minimization of the objective function.

The considered scenario comprises a RIS-assisted downlink with a BS serving $K = 3$ NOMA users. It is assumed that the BS operates at $f_0 = 1$ GHz, and for each user, the RIS observation range is set to 500 m. The remaining simulation parameters are $B = 100$ MHz, $T_s = 916$ K, $A_e^{\mathrm{rx}} = 0.01$ m^2, and $L_s = 40$ dB. Moreover, in the simulations, a residual interference factor of 10^{-3} is considered for numerical stability as well as to model imperfect SIC. Finally, the minimum PAP for all users, $PAP_{\min_i}$, $i = 1, \dots, K$, is set to 0 W·m^2.

In the considered scenario, the spectral efficiency from (9) for the three NOMA users is shown in Fig. 2 as a function of range, assuming PAP values of $\{20, 10, 5\}$ mW·m^2 for the users. In the figure, the corresponding range limit for each user is also indicated. QoS values beyond these limits are set to zero. The target spectral efficiency ($C^\star = 1$ bps/Hz) is highlighted as well. The corresponding range values $R^\star$ for each user are then obtained by numerically solving $C(R) - C^\star = 0$ with respect to $R^\star$.

Fig. 3(a) shows the quality metric as a function of the RIS partition assigned to each user. As expected, increasing the allocated RIS partition improves quality until the range limit is reached, after which additional elements provide negligible gains. For the considered parameter settings, the three curves are nearly overlapping.

Fig. 3(b) shows the utility function from (12) for different values of the parameter $\xi = \{0.5, 0.7, 1, 1.3, 1.5\}$. The objective and threshold ranges for the three NOMA users are

This article has been accepted for publication in IEEE Networking Letters. This is the author's version which has not been fully edited and content may change prior to final publication. Citation information: DOI 10.1109/LNET.2026.3737598

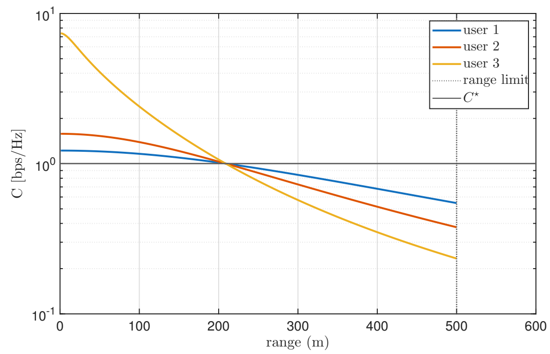

Fig. 2. Spectral efficiency (bps/Hz) for each RIS-assisted NOMA user, assuming an initial PAP allocation of $\{20, 10, 5\}$ mW·m^2 for the three users.

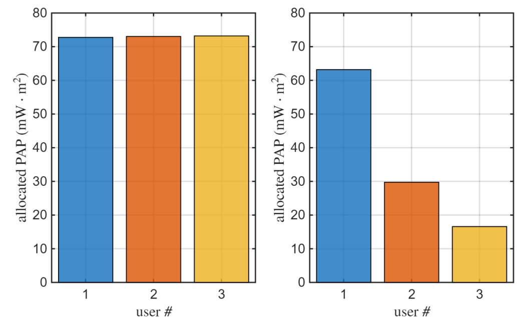

Fig. 4. PAP allocation resulting from RIS partitioning for three NOMA users. The left figure corresponds to nominal operational conditions, while the right figure shows the optimized allocation obtained with priority weights $\boldsymbol{w} = [0.5, 0.3, 0.2]^T$.

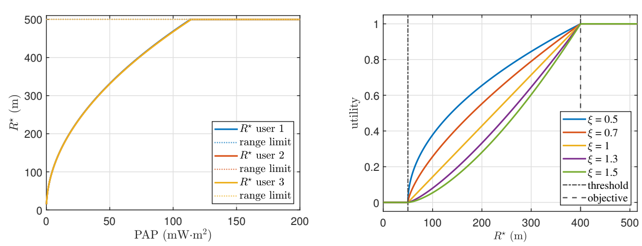

(a) (b)

Fig. 3. Quality metric and utility function. Subplot (a) depicts the Quality metric as a function of the allocated RIS partition for the different users. Subplot (b) shows the utility function versus quality metric $R^\star$ for different values of the exponent ξ.

set to $R_o = 400$ m and $R_t = 50$ m, respectively, which can be adjusted according to the specific requirements. Communication is considered valid within a segment defined by two concentric circles centered at the allocated RIS elements, from a minimum distance corresponding to the RIS allocation up to the maximum range of interest, determining the maximum achievable utility. The curves illustrate the utility function behavior before and after the threshold and objective ranges, as well as the effect of the exponent ξ, which emphasizes values closer to either the objective or the threshold. In the following simulations, ξ is set to 0.7 for all users.

The first simulation considers RIS partitioning under nominal operational conditions (i.e., without optimization), where each user achieves its maximum utility. In this case, every user uses all required RIS elements (maximum utility PAP) to satisfy its nominal spectral efficiency objective. Fig. 4 (left side) illustrates this distribution with a bar chart of the PAP allocated to each user. The maximum utility is obtained with $\boldsymbol{PAP} = [72.7, 73.0, 73.2]^T$ mW·m^2, resulting in a total PAP of approximately 218.96 mW·m^2, i.e., the sum of the individual maximum utility allocations.

Comparing the bar chart in the left-hand side of Fig. 4 with the utility-versus-resource curves in Figs. 3(a)-(b), it is evident that under nominal conditions all users achieve their maximum utility, with the quality metric for each user meeting or exceeding its target. In realistic scenarios, however, the total RIS resources may be insufficient to assign the ideal PAP to every user, as some resources must be reserved for other communication tasks, as well as for their mutual interference. Consequently, the RIS controller must compute an optimal PAP allocation subject to a maximum PAP budget.

In the considered case study, the maximum available PAP is set to 50% of that required under nominal operational conditions, i.e., 109.5 mW·m^2. Furthermore, the priority weight vector is set to $\boldsymbol{w} = [0.5, 0.3, 0.2]^T$, assigning lower priority to the user experiencing the best channel conditions. Solving Problem $\mathcal{P}$ under these constraints yields the solution shown on the right-hand side of Fig. 4, corresponding to the PAP allocation $\boldsymbol{PAP} = [63.2, 29.7, 16.6]^T$ mW·m^2.

To further interpret these results, Fig. 5 reports, for each NOMA user, the optimal PAP allocation as a function of the corresponding $R^\star$, together with the achieved utility. As expected, the RIS controller assigns a larger portion of the available PAP to user 1, which has the highest priority, resulting in $R^\star = 372.8$ m and the largest utility value. Similarly, user 2 attains a relatively high utility with $R^\star = 255.1$ m due to its intermediate priority weight (0.3). Conversely, the lowest performance is observed for user 3, for which the allocated PAP yields a utility of only 0.53, owing to its lower priority weight of 0.2. Finally, the proposed approach is compared with a conventional static PAP allocation strategy, adopted as the reference benchmark. Under the static allocation, the achieved spectral efficiencies are $C_k = \{0.44, 0.64, 1.19\}$ bps/Hz, revealing an unbalanced performance across users. In contrast, the proposed optimization yields $C_k = \{0.88, 0.73, 0.66\}$ bps/Hz, reducing the disparity among users and providing a more balanced allocation that better accommodates heterogeneous QoS requirements. These results highlight the benefit of dynamically optimizing the PAP allocation according to user-specific utility functions rather than relying on uniform resource partitioning. It is worth emphasizing that the proposed framework redistributes the available PAP to maximize the overall system utility while accounting for heterogeneous QoS requirements. As a result, although both approaches achieve a similar aggregate spectral efficiency, the proposed solution provides a considerably more balanced distribution of spectral efficiency among users.

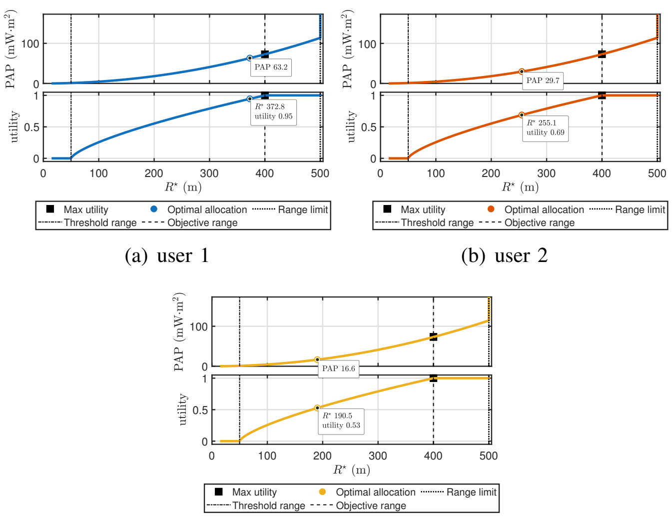

(a) user 1 (b) user 2 (c) user 3

Fig. 5. Optimized RIS partitioning and corresponding utility for the three NOMA users (subplots a)-c)), with priority weights $\boldsymbol{w} = [0.5, 0.3, 0.2]^T$.

V. Conclusions

This letter presented a framework for efficient RIS partitioning in downlink RIS-assisted NOMA systems. By dividing the RIS into multiple sub-surfaces assigned to different users, the approach reduces optimization complexity and mitigates interference in challenging propagation conditions. Utility-based metrics were used to capture individual user requirements, and the resulting constrained optimization problem was solved numerically. Simulation results confirm the validity of the proposed strategy. Future works may extend the framework to uplink scenarios, as well as multi-cell deployments.

VI. Acknowledgment

The author thanks Dr. G. Manfreda for the support in some preliminary simulations during his MSc thesis at University of Basilicata.

References

[1] F. Liu, Y. Cui, C. Masouros, J. Xu, T. X. Han, Y. C. Eldar, and S. Buzzi, “Integrated Sensing and Communications: Towards Dual-Functional Wireless Networks for 6G and Beyond,” *IEEE Journal on Selected Areas in Communications*, vol. 40, no. 6, pp. 1728–1767, 2022.

[2] T. A. Zewde and M. C. Gursoy, “NOMA-Based Energy-Efficient Wireless Powered Communications,” *IEEE Transactions on Green Communications and Networking*, vol. 2, no. 3, pp. 679–692, 2018.

[3] R. Valentini, P. Di Marco, and F. Santucci, “A NOMA Scheme for IoT Enabled by Selective Powering of Passive Backscattering Nodes,” *IEEE Communications Letters*, vol. 26, no. 9, pp. 2195–2199, 2022.

[4] M. Di Renzo, A. Zappone, M. Debbah, M.-S. Alouini, C. Yuen, J. de Rosny, and S. Tretyakov, “Smart Radio Environments Empowered by Reconfigurable Intelligent Surfaces: How It Works, State of Research, and The Road Ahead,” *IEEE Journal on Selected Areas in Communications*, vol. 38, no. 11, pp. 2450–2525, 2020.

[5] D. Ciuonzo, A. Zappone, M. Di Renzo, and L. Wu, “Massive MIMO Channel-aware Decision Fusion Aided by Reconfigurable Intelligent Surfaces,” in *2025 IEEE International Conference on Acoustics, Speech and Signal Processing (ICASSP)*, 2025, pp. 1–5.

[6] G. Yang, X. Xu, Y.-C. Liang, and M. Di Renzo, “Reconfigurable Intelligent Surface-Assisted Non-Orthogonal Multiple Access,” *IEEE Transactions on Wireless Communications*, vol. 20, no. 5, pp. 3137–3151, 2021.

[7] P. Di Marco, R. Valentini, F. Santucci, G. Pettanice, and G. Antonini, “Boosting NOMA Systems Through Smart Metasurfaces,” *Frontiers in Communications and Networks*, vol. 3, 2022.

[8] Y. Liu, X. Mu, X. Liu, M. Di Renzo, Z. Ding, and R. Schober, “Reconfigurable Intelligent Surface-Aided Multi-User Networks: Interplay Between NOMA and RIS,” *IEEE Wireless Communications*, vol. 29, no. 2, pp. 169–176, 2022.

[9] D. Sarkar, Yogita, S. S. Yadav, V. Pal, N. Kumar, and S. K. Patra, “A Comprehensive Survey on IRS-Assisted NOMA-Based 6G Wireless Network: Design Perspectives, Challenges and Future Directions,” *IEEE Transactions on Network and Service Management*, vol. 21, no. 2, pp. 2539–2562, 2024.

[10] L. Pallotta and P. Di Marco, “Uplink Sum-Rate Optimization in RIS-Assisted NOMA Systems via Conjugate Gradient Descent Method,” *IEEE Open Journal of the Communications Society*, vol. 6, pp. 9764–9774, 2025.

[11] Y. Ata, C. Leoni, and A. M. Vegni, “Time Switching-Variable Mode Splitting Protocol for STAR-RIS-aided SWIPT in NOMA Networks,” *IEEE Transactions on Communications*, vol. 74, pp. 247–260, 2026.

[12] C. Cai, X. Yuan, and Y.-J. A. Zhang, “RIS Partitioning Based Scalable Beamforming Design for Large-Scale MIMO: Asymptotic Analysis and Optimization,” *IEEE Transactions on Wireless Communications*, vol. 22, no. 9, pp. 6061–6077, 2023.

[13] Y. Gevez, E. Arslan, and E. Basar, “A Supervised Learning-Assisted Partitioning Solution for RIS-Aided NOMA Systems,” *IEEE Transactions on Cognitive Communications and Networking*, vol. 10, no. 4, pp. 1430–1440, 2024.

[14] Y. Gevez, Y. I. Tek, and E. Basar, “Dynamic RIS Partitioning in NOMA Systems using Deep Reinforcement Learning,” *Frontiers in Antennas and Propagation*, vol. 2, no. 1418412, 2024.

[15] X. Wang, R. Zheng, F. Du, X. Zhao, Y. Zhang, Y. Xu, S. Geng, and P. Qin, “Joint Beamforming and Reflecting Elements Optimization for Segmented RIS Assisted Multi-User Wireless Networks,” *IEEE Transactions on Vehicular Technology*, vol. 73, no. 3, pp. 3820–3831, 2024.

[16] M. Makin, S. Arzykulov, A. Celik, A. M. Eltawil, and G. Nauryzbayev, “Optimal RIS Partitioning and Power Control for Bidirectional NOMA Networks,” *IEEE Transactions on Wireless Communications*, vol. 23, no. 4, pp. 3175–3189, 2024.

[17] C. Leoni and A. M. Vegni, “RIS Partitioning-aided Multi-User Communications in Asymmetric RF/VLC Indoor Systems,” *IEEE Transactions on Mobile Computing*, pp. 1–17, 2025.

[18] Y. Gevez, A. Khaleel, and E. Basar, “A Novel Partitioning Scheme for RIS Identification and Beamforming,” *IEEE Wireless Communications Letters*, vol. 15, pp. 245–249, 2026.

[19] A. Charlish and F. Hoffmann, “Cognitive Radar Management,” *Novel Radar Techniques and Applications: Waveform Diversity and Cognitive Radar, and Target Tracking and Data Fusion*, vol. 2, pp. 157–193, 2017.

[20] A. Aubry, A. De Maio, and L. Pallotta, “Power-Aperture Product Resource Allocation for Radar ISAC,” in *2023 IEEE International Workshop on Technologies for Defense and Security (TechDefense)*, 2023, pp. 352–357.

[21] A. Aubry, A. De Maio, and L. Pallotta, “Power-Aperture Resource Allocation for a MPAR With Communications Capabilities,” *IEEE Transactions on Vehicular Technology*, vol. 73, no. 6, pp. 7474–7488, 2024.

[22] “Quality-of-Service Optimization for Radar Resource Management,” https://it.mathworks.com/help/radar/ug/quality-of-service-optimization-for-resource-management-in-multifunction-phased-array-radar.html, Mathworks Matlab.

[23] D. Tse and P. Viswanath, *Fundamentals of Wireless Communication*. Cambridge University Press, 2005.

[24] M. Chiang, “To Layer or not to Layer: Balancing Transport and Physical Layers in Wireless Multihop Networks,” in *IEEE INFOCOM 2004*, vol. 4, 2004, pp. 2525–2536.

[25] F. Hoffmann and A. Charlish, “A Resource Allocation Model for the Radar Search Function,” in *2014 International Radar Conference*. IEEE, 2014, pp. 1–6.

[26] “Find minimum of constrained nonlinear multivariable function,” https://it.mathworks.com/help/optim/ug/fmincon.html?s_tid=doc_ta, Mathworks Matlab.

[27] R. H. Byrd, J. C. Gilbert, and J. Nocedal, “A Trust Region Method Based on Interior Point Techniques for Nonlinear Programming,” *Mathematical programming*, vol. 89, pp. 149–185, 2000.